Supporting Information

Evaluating the phase-dependent electrocatalytic activity of manganese phosphides for hydrogen evolution reaction

Kyeong-Ho Kim[1,2,†], Yoo Sei Park[3,4,†], Jong Min Lee[5,†], Min Ho Seo[6,], Seong-Hyeon Hong[1,*] and Sung Mook Choi[3,7,*]*

Affiliation

[1]Department of Materials Science and Engineering and Research Institute of Advanced Materials, Seoul National University, Seoul 151-744, Republic of Korea

[2]Department of Materials Science and Engineering, Pukyong National University, Busan 48513, Republic of Korea

[3]Department of Hydrogen Energy Materials, Surface & Nano Materials Division, Korea Institute of Materials Science (KIMS), Changwon 51508, Republic of Korea

[4]Department of Advanced Material Engineering, Chungbuk National University, 1 Chungdae-ro, Seowon-gu, Cheongju, Chungbuk 28644, Republic of Korea

[5]Fuel Cell Research & Demonstration Center, Hydrogen Energy Research Division, Korea Institute of Energy Research, Buan-gun 56332, Republic of Korea

[6]Department of Nanotechnology Engineering, Pukyong National University, Busan 48547, Republic of Korea

[7]Advanced Materials Engineering, University of Science and Technology (UST), Daejeon 34113, Republic of Korea

[†]These authors contributed equally to this work.

* Corresponding author
Dr. Sung Mook Choi, Prof. Seong-Hyeon Hong, Prof. Min Ho Seo

E-mail: akyzaky@kims.re.kr, shhong@snu.ac.kr, foifrit@pknu.ac.kr

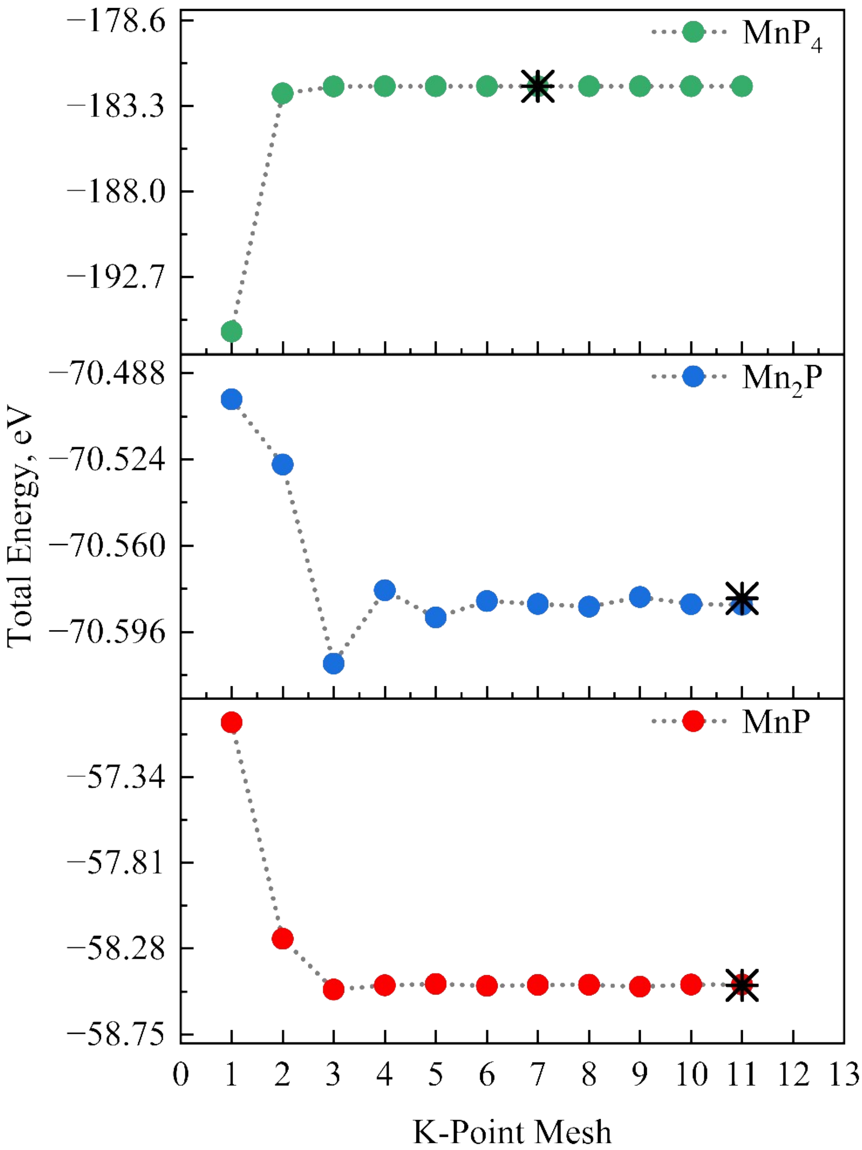

Fig. S1. Energy convergence with k-point mesh for MnP (red), Mn_2P (blue), and MnP_4 (green). Black markers indicate k-points used for bulk optimization

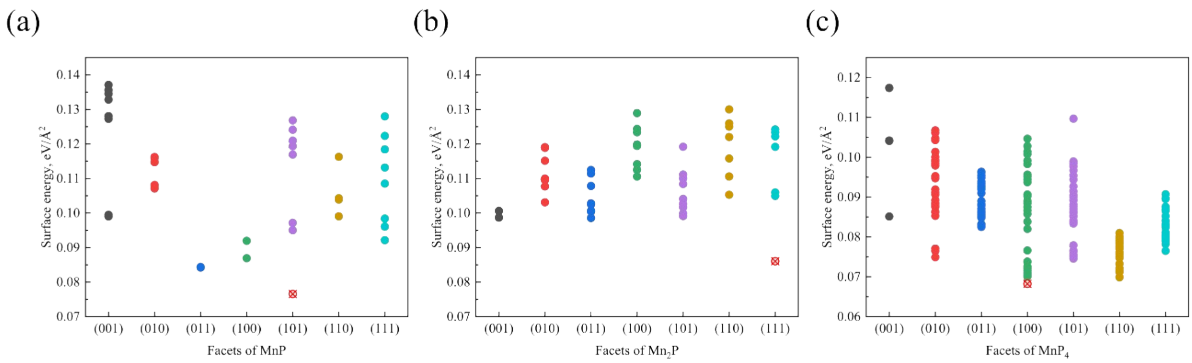

Fig. S2. Surface energies of various facets of MnP, Mn_2P, and MnP_4. Surface energies (eV/Å²) for different low-index facets of (a) MnP, (b) Mn_2P, and (c) MnP_4, respectively.

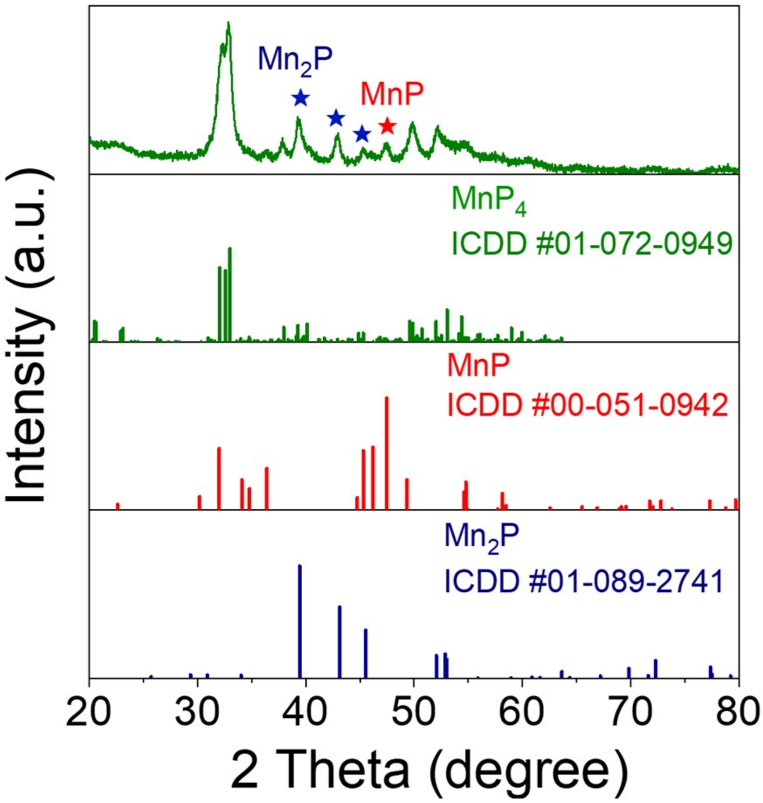

Fig. S3. The XRD pattern of as-milled powders with Mn and P (1:4) for 20 h. The reference peaks for Mn_2P (ICDD # 01-089-2741, blue solid line), MnP (ICDD # 00-051-0942, red solid line), and MnP_4 (ICDD # 01-072-0949, green solid line) are included.

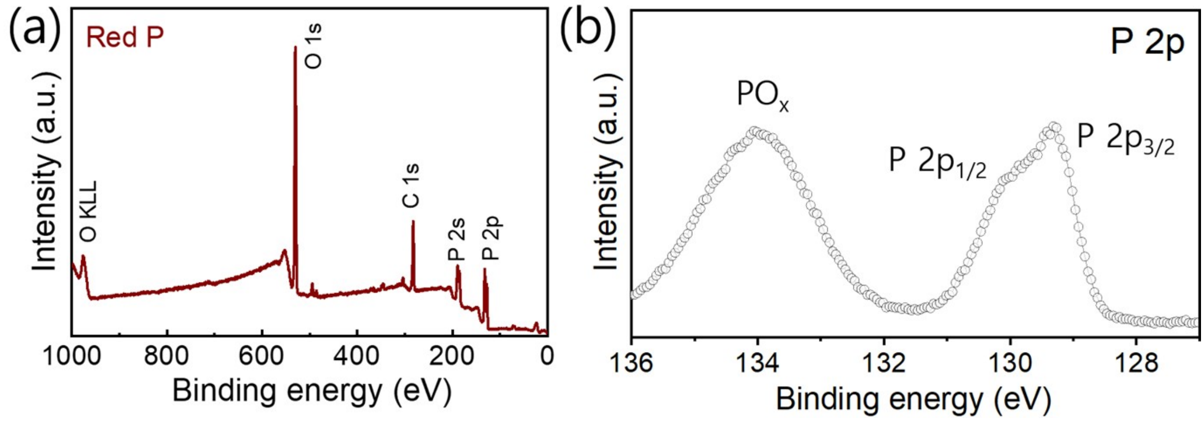

Fig. S4. XPS spectra of commercial red phosphorus for (a) survey and (b) P 2p, respectively.

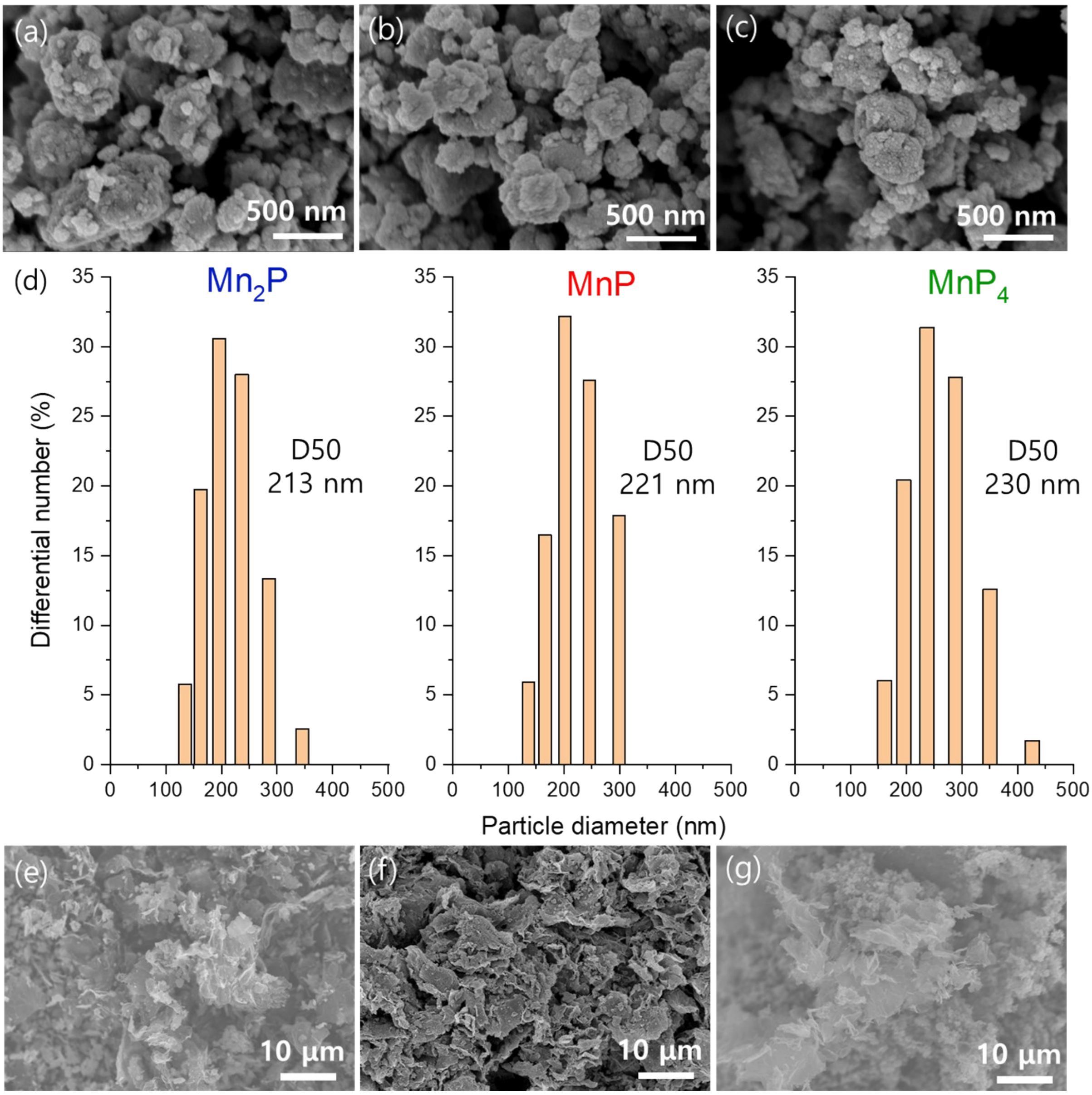

Fig. S5. SEM images of as-prepared (a) Mn_2P, (b) MnP, and (c) MnP_4 nanoparticles, respectively, and (d) their particle size distributions. SEM images of (e) Mn_2P/Gr, (f) MnP/Gr, and (g) MnP_4/Gr nanocomposites, respectively.

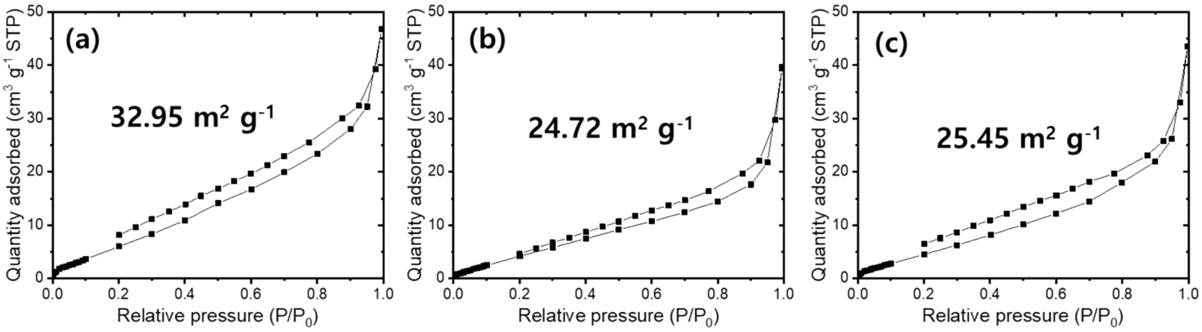

Fig. S6. BET nitrogen adsorption isothermal graphs for the determination of the specific surface areas for (a) Mn_2P, (b) MnP, and (c) MnP_4 nanoparticles, respectively.

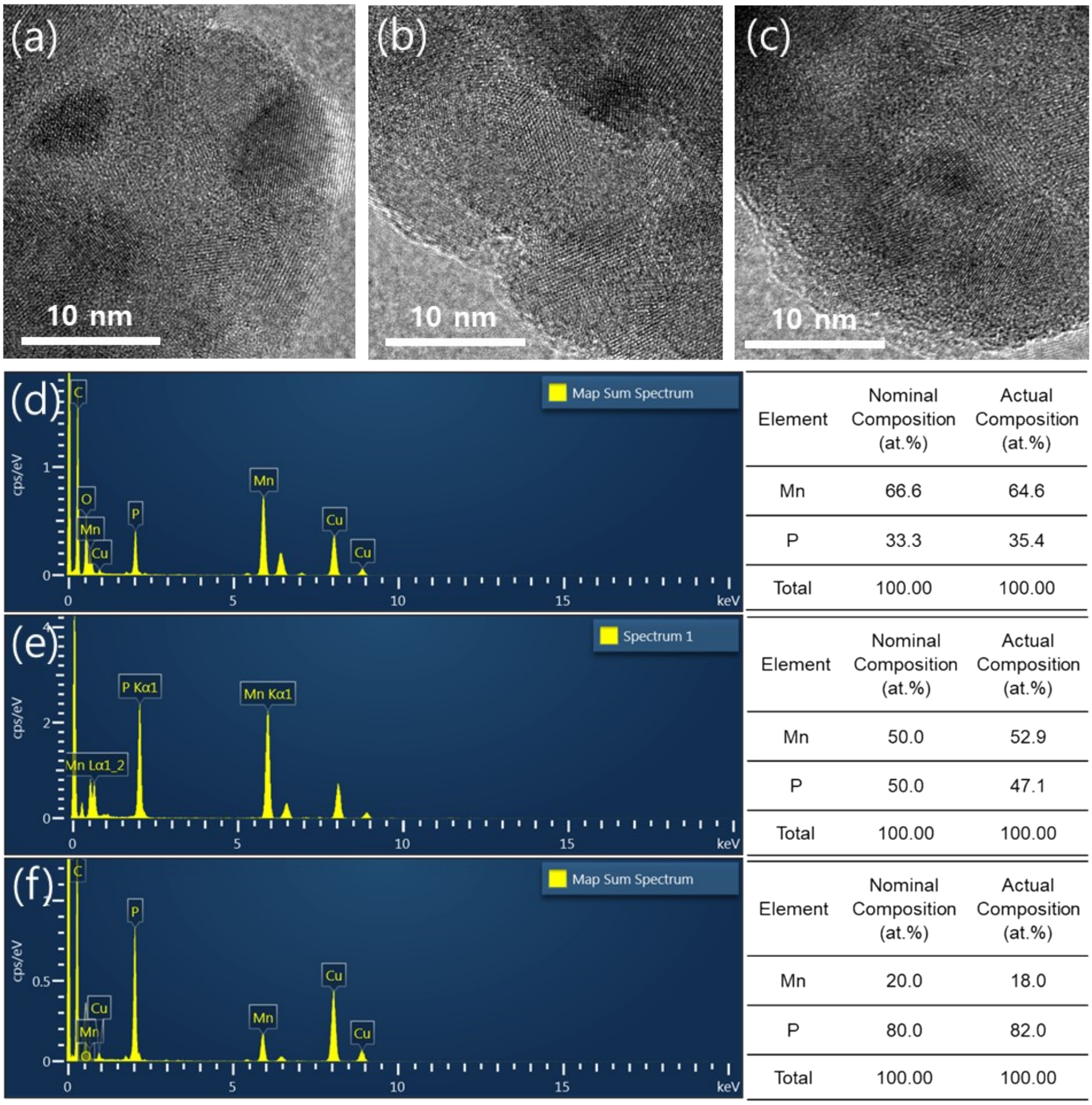

Element	Nominal Composition (at.%)	Actual Composition (at.%)
Mn	66.6	64.6
P	33.3	35.4
Total	100.00	100.00

Element	Nominal Composition (at.%)	Actual Composition (at.%)
Mn	50.0	52.9
P	50.0	47.1
Total	100.00	100.00

Element	Nominal Composition (at.%)	Actual Composition (at.%)
Mn	20.0	18.0
P	80.0	82.0
Total	100.00	100.00

Fig. S7. Low magnification TEM images of (a) Mn_2P, (b) MnP, and (c) MnP_4 nanoparticles, respectively, and EDS spectra and detected compositions for as-prepared (d) Mn_2P/Gr, (e) MnP/Gr, and (f) MnP_4/Gr nanocomposites, respectively.

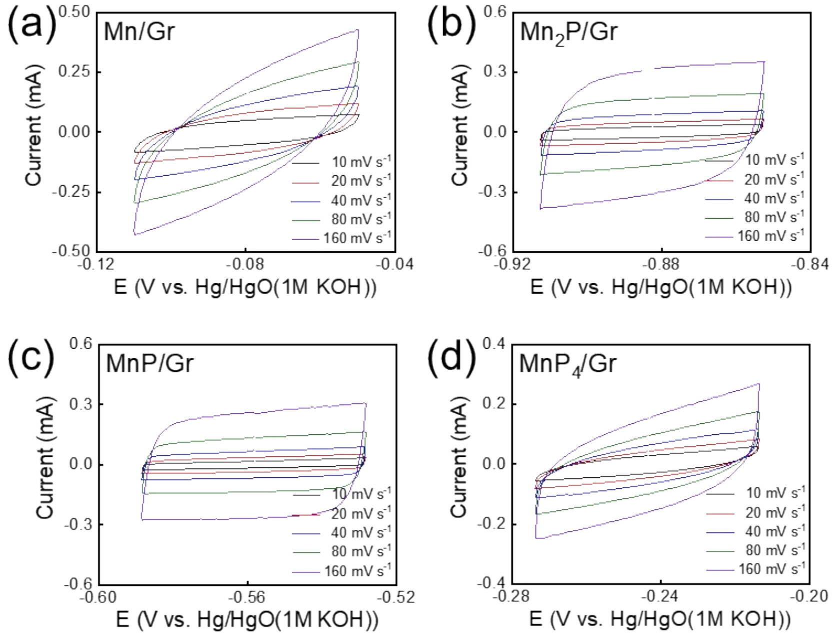

Fig. S8. Cyclic voltammetry of (a) Mn/Gr, (b) Mn_2P/Gr, (c) MnP/Gr, and (d) MnP_4/Gr nanocomposites in non-faradaic region with different scan rates (10, 20, 40, 80, and 160 mV s^{-1}) measured in 1 M KOH.

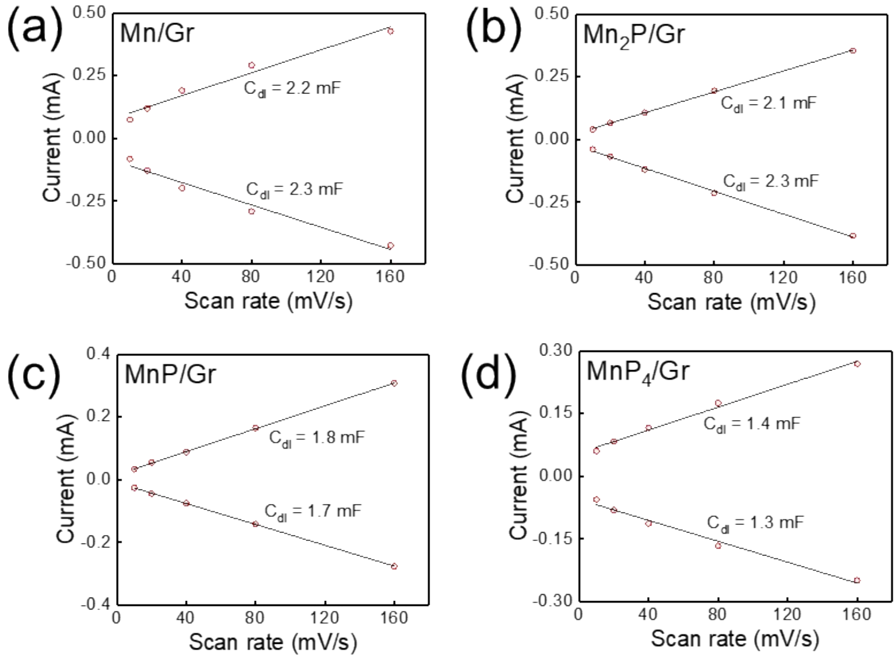

Fig. S9. Double layer capacitance (C_{dl}) of (a) Mn/Gr, (b) Mn_2P/Gr, (c) MnP/Gr, and (d) MnP_4/Gr nanocomposites.

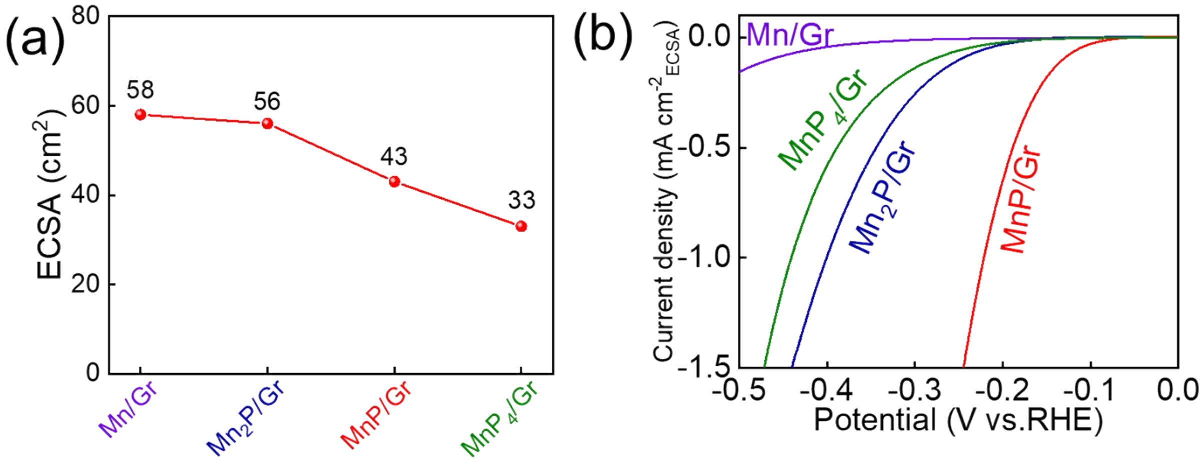

Fig. S10. (a) Electrochemically active surface areas (ECSAs) and (b) HER polarization curves normalized by ECSA of Mn/Gr, Mn_2P/Gr, MnP/Gr, and MnP_4/Gr nanocomposites.

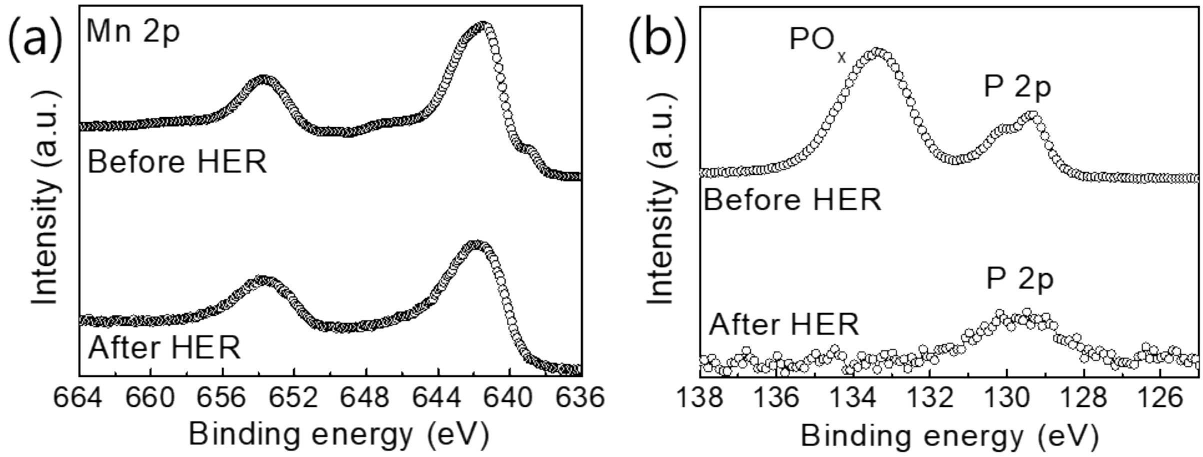

Fig. S11. XPS spectra of MnP/Gr electrodes before and after HER for (a) Mn 2p and (b) P 2p, respectively.

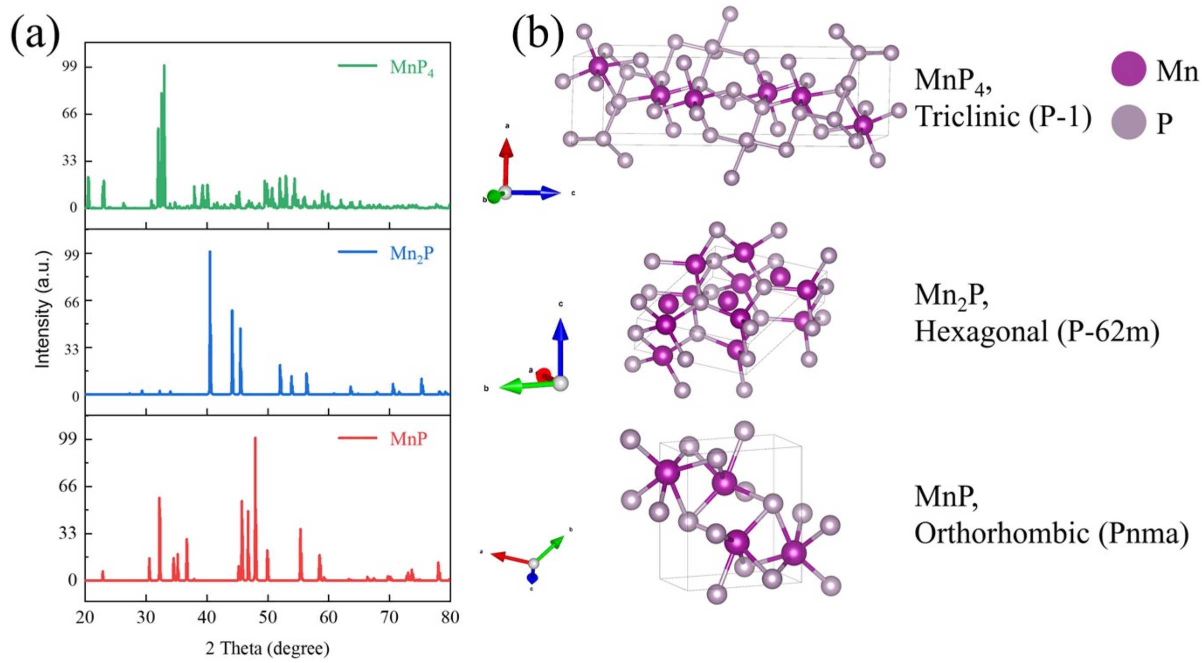

Fig. S12. (a) XRD patterns calculated by DFT and (b) crystal structure illustrations of MnP, Mn_2P, and MnP_4 phases.

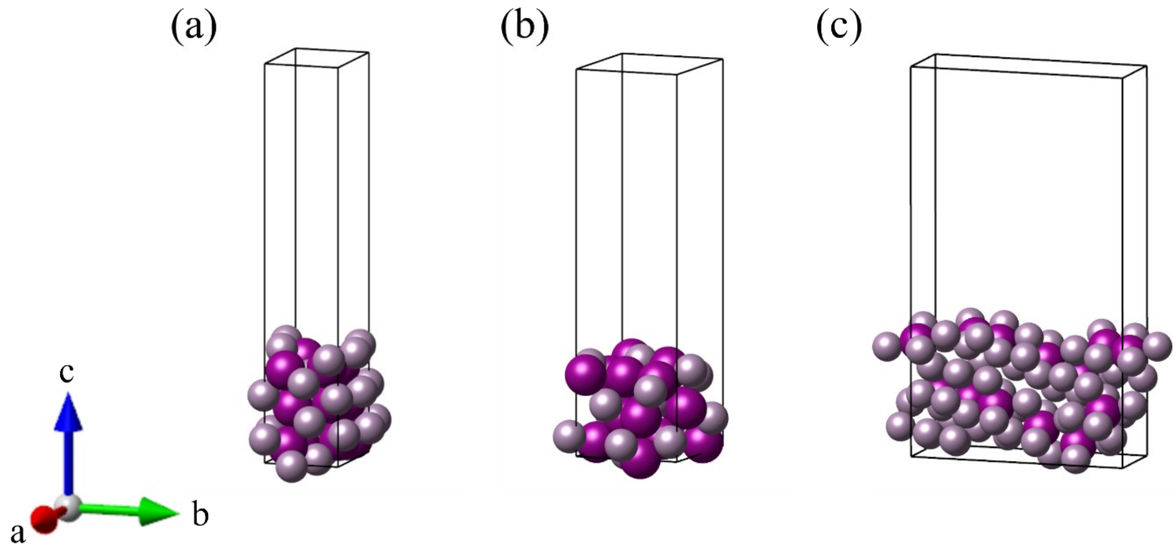

Fig. S13. Crystal structure illustrations of surface with stable surface energy for (a) MnP (101), (b) Mn_2P (111), and (c) MnP_4 (100), respectively.

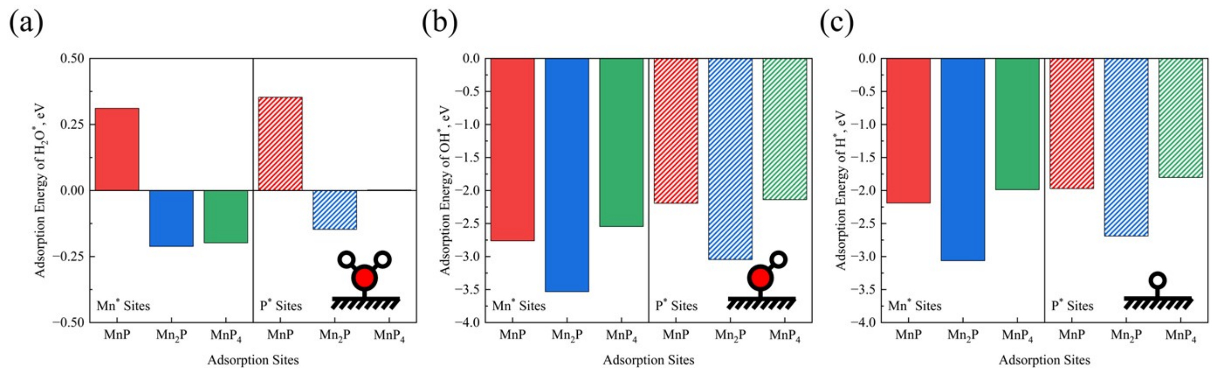

Fig. S14. Adsorption energy of stable hydrogen intermediates on Mn^* and P^* active sites

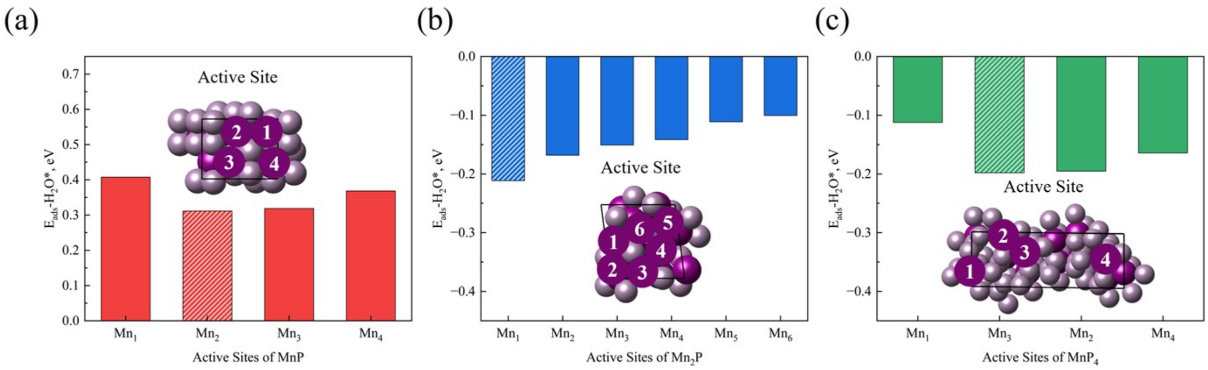

Fig. S15. Adsorption energy of H_2O on (a) MnP, (b) Mn_2P, and (c) MnP_4 surfaces to identify the active sites for the HER.

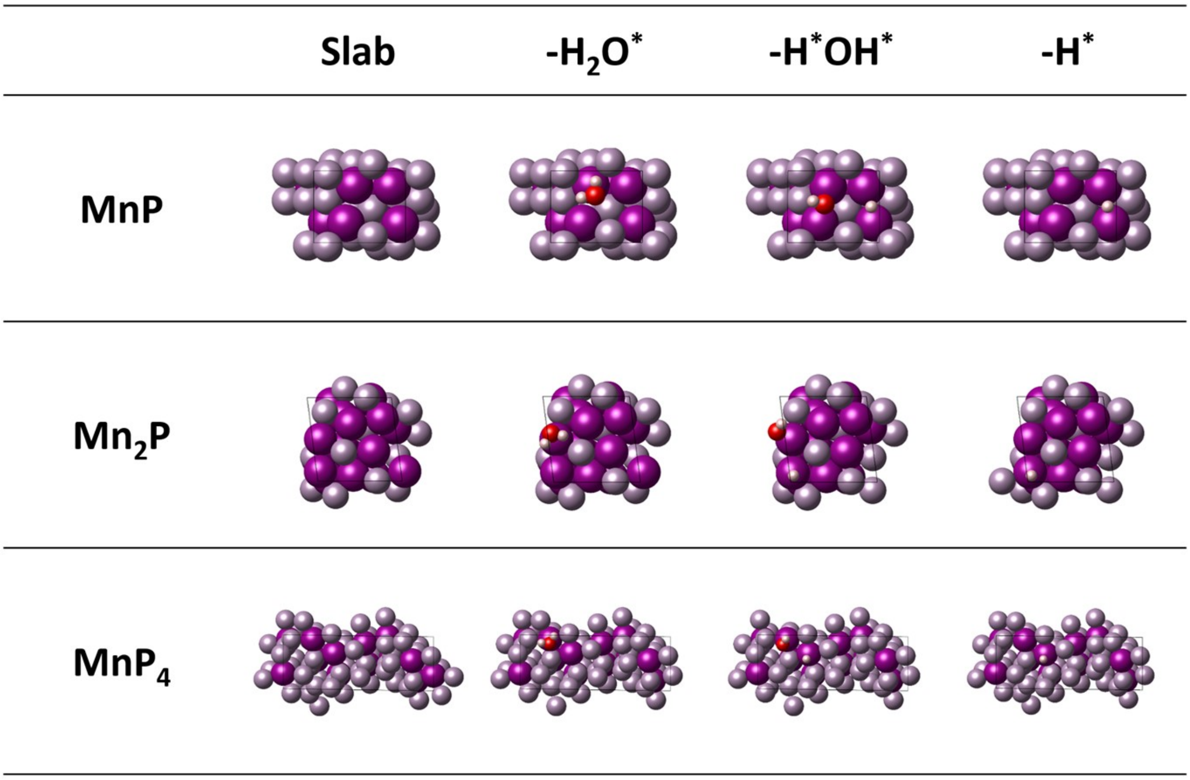

Fig. S16. Schematic HER mechanism on MnP, Mn_2P, and MnP_4 phases.

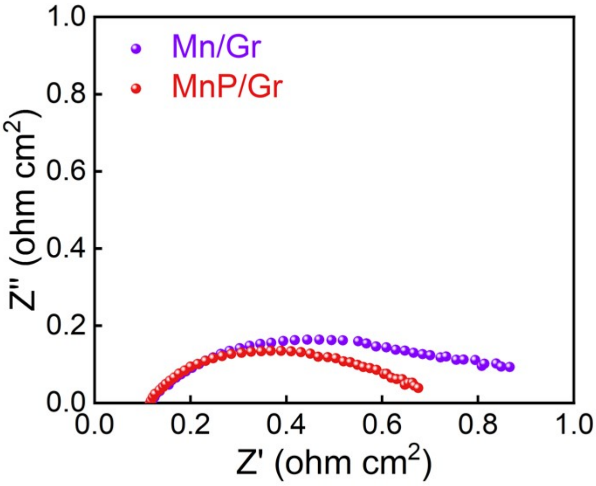

Fig. S17. Nyquist plots of AEM electrolysis cell catalyzed by Mn/Gr and MnP/Gr at a current density of 0.25 A cm^{-2}.

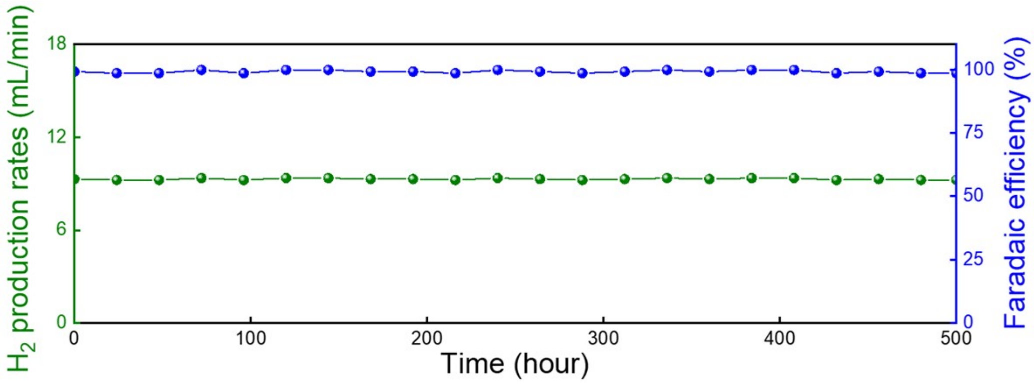

Fig. S18. H_2 production rate and Faradaic efficiency of AEM electrolysis cell catalyzed by MnP/Gr at a current density of 0.25 A cm^{-2}.

Table S1. Nominal and actual compositions determined by ICP-AES of as-prepared Mn_2P/Gr, MnP/Gr, and MnP_4/Gr nanocomposites, respectively.

Compound	Element	Nominal composition (at.%)	Actual composition (at.%)
Mn_2P/Gr	Mn	66.6	65.8
	P	33.3	34.2
MnP/Gr	Mn	50.0	49.3
	P	50.0	50.7
MnP_4/Gr	Mn	20.0	19.8
	P	80.0	80.2

Table S2. The fitted values of R_s and R_{ct} from Nyquist plots for Mn/Gr, Mn_2P/Gr, MnP/Gr, and MnP_4/Gr, respectively.

	Mn/Gr	Mn_2P/Gr	MnP/Gr	MnP_4/Gr
R_s (ohm)	4.49	4.56	4.47	4.43
R_{ct} (ohm)	279.53	15.94	4.75	39.21